



1 **The bacteria-protist link as a main route of dissolved organic**
2 **matter across contrasting productivity areas in the**
3 **Patagonian Shelf**

4

5 Celeste López-Abbate¹, John E. Garzón-Cardona^{1,2}, Ricardo Silva³, Juan-Carlos Molinero⁴,
6 Laura A. Ruiz-Etcheverry^{5,6,7}, Ana M. Martínez⁸, Azul S. Gilabert¹ Rubén J. Lara¹

7

8 ¹ Instituto Argentino de Oceanografía (CONICET-UNS), Camino La Carrindanga km 7.5, 8000 Bahía Blanca,
9 Argentina.

10 ² Universidad Nacional del Sur. Departamento de Química, 8000 Bahía Blanca, Argentina.

11 ³ Instituto Nacional de Investigación y Desarrollo Pesquero (INIDEP), Paseo Victoria Ocampo N°1
12 (B7602HSA), Mar del Plata, Buenos Aires, Argentina.

13 ⁴ Institut de Recherche pour le Développement (IRD), UMR248 MARBEC, IRD/CNRS/IFREMER/UM, Sète
14 Cedex, France.

15 ⁵ Departamento de Ciencias de La Atmósfera y Los Océanos, Facultad de Ciencias Exactas y Naturales,
16 Universidad de Buenos Aires (DCAO, FCEN-UBA), Intendente Guiraldes 2160, Ciudad Universitaria,
17 Pabellón II 2do. Piso, C1428EGA Ciudad Autónoma de Buenos Aires, Argentina

18 ⁶ Centro de Investigaciones Del Mar y La Atmosfera (CIMA/CONICET-UBA), Argentina

19 ⁷ Instituto Franco-Argentino para El Estudio Del Clima y Sus Impactos (IRL-IFAECI/CNRS-CONICET-UBA),
20 Argentina

21 ⁸ Instituto de Química del Sur (INQUISUR-CONICET), Universidad Nacional del Sur, 8000 Bahía Blanca,
22 Argentina.

23

24 Correspondence to: Celeste López-Abbate (mclabbate@iado-conicet.gob.ar)

25



26 **Abstract**

27 While the sources of dissolved organic matter (DOM) in the open ocean are relatively well identified, its fate
28 due to microbial activity is still evolving. Here, we explored how microbial community structure, growth, and
29 grazing of phytoplankton and heterotrophic bacteria influence the DOM pool and the transformation of its
30 fluorescent fraction (FDOM) during dilution experiments in the Patagonian Shelf (SW Atlantic Ocean). This
31 area constitutes a global hotspot of carbon sequestration due to intense biological productivity which peaks at
32 the shelf break front. The productive stations at the shelf break front featured a food web primarily based on
33 phytoplankton and heterotrophic bacteria, while less productive mid-shelf stations showed greater dependence
34 of protistan predators on bacterial biomass. Although phytoplankton biomass was higher than that of bacteria,
35 protists selectively preyed on the latter, which exhibited faster growth rates, denoting high trophic specificity
36 of grazers. Trophic efficiency and omnivory favored a bottom-heavy biomass distribution, characterized by
37 consumer biomass dominance over producers, except in highly productive stations influenced by nutrient-rich
38 upwelling waters, where a typical pyramid structure was observed. Our results showed that in addition to the
39 commonly accepted factors such as phytoplankton growth stage and bacterial community composition, DOM
40 accumulation versus consumption is also linked to bacterial grazing. Intense grazing on heterotrophic bacteria
41 promoted DOM accumulation, likely by reducing the number of active, DOM-consuming bacteria and by
42 providing egestion compounds to the DOM pool. Moreover, bacterial consumption of DOM appeared
43 uncoupled from its total amount but was influenced by FDOM properties. These findings suggest that under
44 high bacterial growth rate that follows the onset of the productive season, protistan grazers act as a link between
45 bacterial biomass and higher trophic levels, partially diverting DOM lysate production by virus.

46

47 **1. Introduction**

48 Marine microbes have consensual impact on human life due to their climate-active role that stems from their
49 ecosystem functions and broad predominance in marine biomass (Cavicchioli et al., 2019). The balance between
50 microbial climate roles, i.e., CO₂ fixation, nutrient regeneration, and carbon sequestration, has consequential
51 buffering effects on the currently unbalanced global carbon cycle (Hutchins and Fu, 2017). The prediction of
52 microbial climate roles, however, requires a deep understanding of microbial interactions since most metabolic
53 outcomes are shaped by both resource supply and mortality sources. Protistan grazers along with viral lysis
54 constitute the main sources of mortality of phytoplankton and prokaryotes in the ocean (Brussaard, 2004; Calbet
55 and Landry, 2004; Weinbauer and Peduzzi, 1995). Both mortality sources create divergent carbon routes as
56 viral lysis directs host biomass toward the dissolved organic matter (DOM) cycle and grazing may repackage
57 bacterial and phytoplankton biomass inaccessible to mesozooplankton and fish larvae thus linking the microbial
58 loop with higher trophic levels (Azam et al., 1983). Protistan grazers further impact element cycle by recycling
59 nutrients, thus prolonging bloom formation (Sherr and Sherr, 2016), and by providing DOM from excretion and
60 egestion (Kujawinski et al., 2004). The consequences of selective grazing upon prokaryotes or phytoplankton,
61 however, are less well understood as it may result from the interplay of various factors. For example, while
62 size-specific grazing prompt compositional shifts in phytoplankton (e.g., Kanayama et al., 2020), the more
63 generalist grazing on bacteria implies that community composition tends to remain more stable under grazing



64 pressure (Baltar et al., 2016). On the other hand, grazing on bacteria seems to remain close to bacterial
65 production, specially under oligotrophic conditions (Sanders et al., 1992), but phytoplankton may temporally
66 scape protistan grazing under favourable growth conditions thus allowing for bloom formation (Irigoien et al.,
67 2005). The trophic transfer efficiency varies between phytoplankton and bacteria-based food webs, with the
68 former typically involving fewer carbon steps before reaching microcrustaceans (Berghlund et al., 2007).
69 DOM represents the ocean's second most significant carbon reservoir after dissolved inorganic carbon, and its
70 characteristics undergo alterations due to physical and biological processes on a daily basis (Spencer et al.,
71 2007). The optical properties of DOM offer insights into its biochemical characteristics. The chromophoric
72 fraction indirectly estimates phytoplankton DOM production (Romera Castillo et al., 2010), while fluorescence
73 serves as an indicator of its biological and photochemical reactivity (Stedmon et al., 2003). While phytoplankton
74 is the primary source of DOM in the ocean, other processes such as viral lysis and grazing also significantly
75 influence its magnitude and complexity. The impact of protistan grazing on carbon pools, is driven by the
76 remineralization of organic carbon and by the formation of DOM by reworking phytoplankton and bacterial
77 biomass (Baña et al., 2014; Lund Paulsen et al., 2019; Nagata and Kirchman, 1992). However, the impact of
78 selective grazing pressure on DOM-transforming prey, i.e., bacteria and phytoplankton, is less well understood.
79 Shelf areas represent global hotspots of carbon transformation not only due to their high productivity but also
80 because of the intense interaction with terrestrial habitats and the local and meso-scale mixing processes
81 connecting the euphotic zone with bottom sediments (Laruelle et al., 2018). The Patagonian Shelf, characterized
82 by highly productive frontal regions, is particularly notable for its substantial potential for carbon absorption
83 on a global scale ($-0.02 \text{ Gt C yr}^{-1}$) (Kahl et al., 2017). The emergence of an acidification rate ranging from -
84 0.001 to -0.0018 per year in the water masses adjacent to the shelf is likely linked to ongoing CO_2 capture
85 processes. In particular, the northern area of the shelf exhibits the lowest pH values, attributed to the heightened
86 rate of remineralization occurring in the coastal region (Orselli et al., 2018). Biological processes have been
87 identified as primary drivers of carbon capture in the shelf area (Kahl et al., 2017; Schloss et al., 2007), with
88 model predictions indicating that a significant portion of autochthonous biogenic material is exported to the
89 open ocean in subduction zones at the confluence of the Brazil and Malvinas currents (Berden et al., 2020;
90 Franco et al., 2018). Despite the recognition of biological mechanisms mediated by microbial food webs as key
91 contributors to carbon capture in the shelf area, the underlying ecological mechanisms remain insufficiently
92 explored.

93 Given that both phytoplankton and bacteria are essential in the processing and accumulation of DOM in the
94 sunlit ocean and that selective grazing upon these groups impact on its subsequent directionality, we conducted
95 dilution experiments to measure growth and grazing of total phytoplankton and bacteria and monitored CDOM
96 and FDOM transformation over the course of the experiments. The aim of this study was to assess the fate of
97 dissolved organic matter (DOM) within the context of naturally occurring ecological interactions between
98 producers (phytoplankton and bacteria) and protistan grazers in two areas of the Patagonian Shelf during spring
99 bloom conditions. The examined areas encompassed both the mid-shelf region, characterized by low to
100 moderate productivity, and the shelf break, an upwelling and productive area known for recurrent spring bloom
101 formation. We found that regardless of productivity level, grazers preyed selectively on bacteria and that grazing



102 pressure on bacteria was a primary factor driving the short-term accumulation of DOM. Our results contribute
103 to better defining the functional roles of protistan grazers in carbon routing within the ocean.

104

105 **2. Material and Methods**

106 **2.1 Sampling strategy**

107 The Patagonian Shelf is one of the largest continental shelf areas in the world and its more conspicuous feature
108 is the presence of a 2500 km-long upwelling front at the shelf break area characterized by recurrent spring
109 blooms and intense geochemical transformation (Romero et al., 2006). Biological carbon fixation in this frontal
110 area contributes substantially to the sequestration of large amounts of carbon and constitutes one of the major
111 CO₂ sinks at the global level (Kahl et al., 2017). Here, we selected two groups of stations in the mid-shelf
112 (stations 23, 22 and 21 from the coast to the open ocean) and the shelf break area (stations 14, 13 and 12 from
113 the coast to the open ocean). Mid-shelf stations were separated by ca. 30 km intercepting the 50 m isobath while
114 shelf break stations were separated by ca. 18 km and intercepted the 100 and 200 m isobaths. According to the
115 bioregionalization of the Patagonian shelf waters proposed by Delgado et al. (2023), mid-shelf stations are
116 located in low to moderate productivity regions (mean chlorophyll-a concentration during the spring peak
117 between 1.14 and 2.48 mg m⁻³), while the shelf break stations are nested in the upwelling, highly productive
118 region (mean chlorophyll-a concentration during the spring peak of 5.8 mg m⁻³). Hydrographic data
119 (temperature, salinity, pressure, and fluorescence) were taken with a CTD profiler SBE 9plus during the cruise
120 H0917 from October 9 to 12, 2017.

121

122 **2.2 Analytical determination of inorganic nutrients and DOC**

123 Water samples for chemical/plankton determinations and experiments, were taken from the chlorophyll-a
124 maximum with 6 l Niskin bottles attached to the CTD rosette, while dissolved organic carbon (DOC) samples
125 were taken in the surface layer (5 m). Water samples aliquots were taken for the analysis of dissolved nutrients.
126 The measurement of inorganic nutrients (NO₂⁻, NO₃⁻ and NH₄⁺, PO₄³⁻, and Si) was carried out by analyzing 50
127 ml aliquots of seawater preserved with HgCl₂ solution (Kattner and Becker, 1991) The concentration of
128 dissolved inorganic nitrogen (DIN) was calculated as the sum of NO₂⁻, NO₃⁻ and NH₄⁺. Filtered (pre-combusted
129 Whatman GF/F glass fiber filters) samples for DOC were collected in pre-combusted 20 ml glass vials and
130 acidified to pH < 2 with H₃PO₄. Filtrates were analyzed using high-temperature (680°C) catalytic oxidation
131 with Al₂O₃ particles containing 0.5% platinum (Pt) in a TOC analyzer (Dohrmann DC-190, CA, USA). The
132 resulting CO₂ was then quantified using non-dispersive linearized infrared gas analysis (Skoog et al., 1997).
133 Potassium hydrogen phthalate solution was used as the calibration standard.

134

135 **2.3 Satellite chlorophyll-a**

136 Moderate Resolution Imaging Spectroradiometer (MODIS) Aqua images of chlorophyll-a concentration were
137 downloaded from the National Aeronautics and Space Administration (NASA) ocean color web site
138 (<https://oceancolor.gsfc.nasa.gov/>). Daily Level 3 (L3) images with a spatial resolution of 4 km were obtained
139 for the period spanning August 2017 to December 2017, capturing the closest pixel to each sampling point.



140 These images were utilized to construct time series data for each station and assess the phytoplankton's growth
141 phase at each location. To minimize the percentage of missing values, we computed the 5-day mean and applied
142 a low-pass filter to remove the variability lower than 28 days.

143

144 **2.4 Experimental set up**

145 Feeding experiments, based on the dilution technique (Landry and Hassett, 1982), were prepared by gently
146 mixing different amounts of unfiltered water and $<0.2 \mu\text{m}$ water (using Whatman polycarbonate filters) in acid-
147 cleaned glass bottles (1 l). Four dilution treatments (D) were prepared: 10%, 40%, 70% and 100% (whole
148 water). An additional treatment consisting of filtered seawater ($<0.7 \mu\text{m}$, using Whatman GF/F glass fiber
149 filters) was set to evaluate chromophoric (CDOM) and fluorescent dissolved organic matter (FDOM)
150 modifications in the absence of protists and grazers. Seawater from each site was obtained from the chlorophyll-
151 a maximum (20-30 m depth), and pre-filtered by a $200 \mu\text{m}$ mesh net to eliminate large, metazoan grazers.
152 Experimental bottles (3 replicates) were daily (24 h) deployed at a deck-incubator (200 l) equipped with
153 continuous in situ water flow and covered with a double knitted mesh fabric ($\sim 215 \text{ g m}^{-2}$) to attenuate the UV
154 radiation. Dissolved inorganic nutrients (N, P and Si) were added to the incubation bottles by assuming a
155 maximum chlorophyll-a concentration in the mid-shelf area of $2 \mu\text{m l}^{-1}$, and in the shelf-break area of $10 \mu\text{m l}^{-1}$
156 (Delgado et al., 2023). The amount of nutrients added followed Calbet and Saiz (2018) to ensure
157 phytoplankton growth at non-limiting conditions. A series of dilution bottles without nutrient addition was set
158 as control treatment.

159

160 **2.5 Phytoplankton and bacterial growth and grazing by phagotrophic protists**

161 Rate estimates of phytoplankton growth (μ) and mortality due to protist phagotrophy (m) were obtained using
162 the equations of Landry and Hassett (1982). While initially intended for measuring phytoplankton growth and
163 mortality, we adapted this method to assess bacterial growth rate and bacterivory. This approach has been
164 demonstrated to be effective and reliable for use with natural bacterial communities in non-oligotrophic regions
165 (Tremaine and Mills, 1987). The method is based on measuring the initial and final concentration of
166 chlorophyll-a (as a proxy of phytoplankton biomass) and bacterial abundance in triplicate dilution series after
167 an incubation period of 24 h. It assumes that protistan grazing rate is a linear function of prey concentration
168 (Holling type I functional response), and can be calculated as follows:

169

$$170 \mu_0 = 1/t \ln P_t/P_0 = \mu - mD$$

171

172 where μ_0 is the apparent growth rate, P_0 and P_t are the phytoplankton concentration at the initial (0) and final
173 (t) conditions, respectively, D is the dilution series. We tested model fit in every experiment.

174

175 **2.6 Plankton abundance and biomass**

176 Subsamples from the initial and final treatments were collected for chlorophyll-a and bacteria abundance
177 analysis. To determine chlorophyll-a, triplicate samples (300 ml) were filtered through GF/F filters and stored



178 at -20°C . Pigments were extracted with 90% acetone for 24 h in the dark at -20°C and then determined
179 spectrophotometrically according to Jeffrey and Humphrey (1975). Triplicate samples of picoplankton (3 ml)
180 and duplicate samples of nanoplankton (100 ml) were fixed with 0.53 ml of glutaraldehyde (f.c. 2 %) and
181 subsequently processed following the methods described by Porter and Feig (1980). Heterotrophic bacteria
182 were quantified by staining 1 ml seawater sample with 4,6-diamidino-2-phenylindole (DAPI) to a final
183 concentration of $3\ \mu\text{g ml}^{-1}$ and collected on black polycarbonate filters (25 mm diameter, $0.2\ \mu\text{m}$ pore size).
184 The enumeration was done with a microscope Nikon Eclipse 80i equipped with a fluorescence lamp at 100X
185 magnification. Heterotrophic bacteria were identified using a UV excitation filter (330-385 nm). Twenty-five
186 images were taken at random points from each polycarbonate filter using a Nikon DXM1200F digital camera
187 and subsequently, every cell in the image was enumerated and sized using the software ImageJ. Bacterial cell
188 volumes were calculated assigning simple geometric shapes to species (coccos, bacillus), and converted into
189 carbon content ($\mu\text{g C l}^{-1}$) by the allometric model according to Simon and Azam (1989).

190 Protist plankton identification and quantification were conducted using light and epi-fluorescence microscopy
191 at the initial treatment stage. The identification of photosynthetic (PNP) and heterotrophic nanoplankton (HNP)
192 was done by a combination of light and epi-fluorescent microscopy. Note that the size categories PNP and HNP
193 include members from nanoplankton ($5\text{-}20\ \mu\text{m}$) and ultraplankton ($>5\ \mu\text{m}$). Prior to cell enumeration, preserved
194 samples (5 ml) were stained with DAPI (f.c. $5\ \mu\text{g ml}^{-1}$) and proflavin (f.c. $5\ \mu\text{g ml}^{-1}$) and collected on black
195 polycarbonate filters (25 mm diameter, $0.2\ \mu\text{m}$ pore size). Most PNP and HNP were identified using a blue
196 excitation filter (450-490 nm) while Cryptophytes were identified using a green excitation filter (480-550 nm).
197 Cell enumeration was done by settling the preserved sample (1-2 ml) in Utermöhl chambers during 24 h. The
198 entire chamber was analyzed under a Wild M20 inverted light microscope. Similarly, the enumeration of
199 phytoplankton and phagotrophic protists in the size fraction $20\text{-}200\ \mu\text{m}$ was done by settling a variable volume
200 ($10\text{-}50\ \text{ml}$, depending on sediment and plankton concentration) of preserved seawater sample (Lugol's iodine)
201 in Utermöhl chambers during 24 h. It is worth mentioning that samples were pre-filtered through a $200\ \mu\text{m}$
202 mesh to exclude larger consumers from our experiments. This procedure may have also removed colony-
203 forming protists. Biomass estimation involved assigning simple geometric shapes to species to quantify cell
204 volume, which was subsequently converted into carbon content ($\mu\text{g C l}^{-1}$) according to Hillebrand et al. (1999).
205 Protistan taxa abundance was visualized by a heatmap (employing the R package *heatmaply*), and taxa was
206 segmented into functional groups to facilitate visualization. A side dendrogram was included to group similar
207 sampling stations by ordering rows (stations) so that the sum of distances between each one will be minimized.
208 Data for ranking rows was normalized to range from 0 to 1. To assess the dominant taxa contributing to station
209 ordination, a biplot based on non-metric Multi-Dimensional Scaling (MDS) was done to evaluate the correlation
210 of taxa on the station ordination using the R package *vegan*.

211

212 **2.7 Production of CDOM and FDOM transformation**

213 Given that protistan grazing impacts on carbon pools, either by remineralizing organic carbon or by contributing
214 with the formation of DOM by reworking phytoplankton and bacterial biomass (Baña et al., 2014; Lund Paulsen
215 et al., 2019), and that these processes add to the isolated effects of phytoplankton growth and bacterial



216 degradation of DOM in natural communities, we estimated the net DOM production and evaluated the fate of
217 biodegradable and biorefractory compounds during the incubations. For this purpose, we measured CDOM and
218 FDOM at the beginning and end of the experiments in the presence (undiluted treatment, prefiltered by 200
219 μm) and absence of protists (undiluted treatment, prefiltered by 0.7 μm). This procedure captured
220 transformation processes within closed systems at the daily basis. Many biotic and abiotic transformation
221 processes occur at the daily timescale. For instance, photodegradation of refractory products occurs within hours
222 (Timko et al., 2015), while experimental observations revealed that significant shifts driven by biological
223 processes were identifiable after 24 h (Lønborg et al., 2010, 2015; Urban-Rich et al., 2004). Furthermore,
224 experimental results revealed that major microbially driven DOM transformation occur within the first 24 h
225 upon their release by phytoplankton (Gruber et al., 2006; Hach et al., 2020). This emphasizes that detectable
226 DOM transformation processes occurring at short-term periods, can provide clues to assess transient DOM
227 trends within specific succession phases of microbial communities. It is worth mentioning that the treatment
228 filtered by 0.7 μm , excluded part of the bacterioplankton community, notably the particle-attached bacteria, and
229 thus may not accurately reproduce the response of natural communities.

230 The optical properties of FDOM were evaluated from emission-excitation matrices (EEM) obtained with a
231 Shimadzu RF-5301 scanning spectrofluorometer with a 150W xenon lamp and a 1 cm quartz cell. Milli-Q water
232 was used as reference and the intensity of the Raman peak was regularly checked. The emission wavelength
233 ranged between 250 nm and 600 nm while the excitation wavelength ranged between 220nm and 370nm. An
234 estimation of dissolved humic-like and protein-like substances was carried out at the wavelengths proposed by
235 Coble (1996). Humic-like fluorophores: FDOM_C, containing mostly highly unsaturated components, at Ex/Em:
236 350/440 nm; FDOM_A, with moderate degree of unsaturation, at Ex/Em: 250/425 nm and FDOM_M, with low
237 degree of unsaturation, at Ex/Em:310/380 nm. Protein-like fluorophores: FDOM_T, with fresh components, at
238 Ex/Em: 270/330 nm and FDOM_B, corresponding to DOM transformed by biological or physicochemical
239 factors, at Ex/Em: 260/300 nm. Fluorescence intensity of fluorophores was expressed in Arbitrary Units (AU).
240 Fluorophores were identified using the PARAFAC multivariate algorithm (Stedmon and Bro, 2008) and
241 different biogeochemical indicators such as humification index (HIX), fluorescence index (FI), and freshness
242 index (BIX), were calculated (Coble, 1996). The HIX serves as a tool for assessing the diagenetic condition of
243 DOM, as it increases with aromaticity (Bai et al., 2015), while the FI distinguishes between DOM of different
244 origins, i.e., terrestrial vs. microbial (McKnight et al., 2001). BIX aims to estimate the relative contribution of
245 DOM produced in situ by microbes (Huguet et al., 2009).

246 CDOM was measured as the absorbance spectra between 240 to 800 nm measured in a Perkin Elmer Lambda
247 35 spectrophotometer. The absorbance at 254 nm (a_{254}) was used as a proxy of total DOM in the UV spectrum
248 (Brandstetter et al., 1996). Net DOM production was calculated as $1/t \ln(a_{254}t/a_{254}0)$, where $(a_{254})_0$ and
249 $(a_{254})_t$ are the absorbance at 254 nm of CDOM at the initial (0) and final (t) conditions, respectively. Lee et al.
250 (2018) identified parameters with more than a 50% absolute percent difference between the control and treated
251 samples as reliable indicators to distinguish between DOM transformation caused by biodegradation, UV
252 irradiance, and adsorption. Here we used the tendency during incubation of BIX, HIX, FI, and the ratio between
253 FDOM components M and A ($\text{FDOM}_M/\text{FDOM}_A$) as reliable parameters for the discrimination of



254 biodegradation versus UV photodegradation or adsorption. Pairwise relationship between net production of
255 DOM in the presence and absence of protists with variables of interest, was evaluated by simple regression
256 models. The same procedure was used with other variables to test for pairwise relationships of ecological
257 significance.

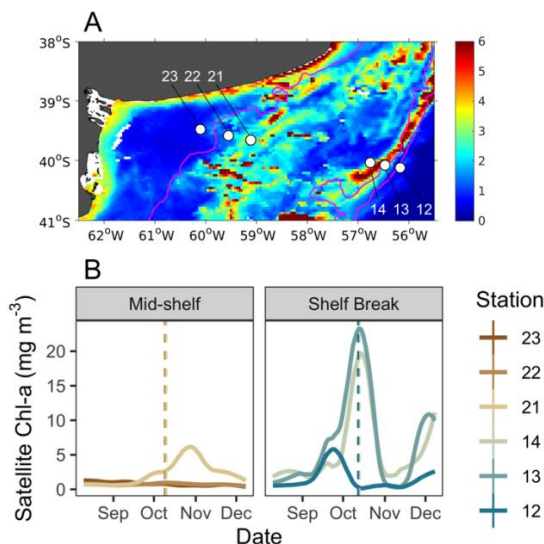
258

259 3. Results

260 3.1 Phytoplankton phenological stages at the sampling area

261 Mean surface chlorophyll-a, derived from satellite observations during the sampling period (October 9-12,
262 2017, Fig. 1a), revealed a band of high phytoplankton concentration at the shelf break, centred at the 114 m
263 isobath in the latitudinal band at 40°S. While the spring bloom typically begins during September in the
264 latitudinal range of our sampling area (Delgado et al., 2023), phytoplankton at the time of sampling, as estimated
265 from satellite chlorophyll-a, were at different phenological stages in each station (Fig. 1b). At the mid-shelf,
266 station 21 showed the highest concentration of satellite chlorophyll-a and the phytoplankton community was at
267 the pulse initiation. Stations 22 and 23 showed lower chlorophyll-a and were sampled at bloom stationary phase.
268 At the shelf break, satellite-derived chlorophyll-a levels were elevated in stations 13 and 14, indicating
269 proximity to the bloom peak, whereas station 12 exhibited low chlorophyll-a concentrations, corresponding to
270 the bloom termination phase.

271



272

273 **Figure 1.A.** Map of the study site showing the location of sampling stations and the mean surface

274 **distribution of satellite chlorophyll-a (MODIS-AQUA) during the sampling period (October 09-12). B.**

275 **Temporal evolution of surface satellite chlorophyll-a concentration at grid points closest to sampling**

276 **stations. Solid lines denote satellite chlorophyll-a concentration at each station, while dotted lines**



277 represent the moment of in situ sampling. Lines are color-coded according to the points representing
 278 each station.

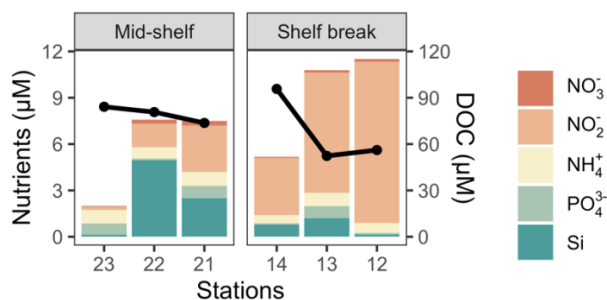
279

280 3.2 Hydrography, nutrients, and DOM properties

281 Thermohaline signature was in the range of the Subantarctic Shelf waters ($33.5 < S < 34$) from station 21 to
 282 station 14 in agreement with Berden et al. (2020) and Ferronato et al. (2023). At the mid-shelf area, station 23
 283 and 22 showed relative higher salinity water ($S > 33.7$), linked to the coastal maximum salinity waters originated
 284 at San Matias Gulf (Lucas et al., 2005). These stations also showed weak stratification, while the rest of the
 285 stations showed a sharper thermocline. The mixed layer depth (MLD) ranged between 10 (stations 12 and 23)
 286 and 31 m (stations 13 and 22). Stations 14 and 21 showed intermediate MLD of 30 and 28 m respectively. All
 287 samples taken at the chlorophyll-a maximum were positioned within the mixed layer.

288 The concentration of dissolved nutrients (DIN, PO_4^{3-} and Si) was highest at station 14 while the lower total
 289 nutrient concentration was recorded at station 23 (Fig. 2a). The primary nitrogen source was NO_3^- , except for
 290 station 22 where NH_4^+ predominated. The only notable distinction between station groups was the concentration
 291 of NO_3^- , which averaged $1.2 \mu\text{M}$ in the mid-shelf stations and $7.3 \mu\text{M}$ in the shelf-break stations. According to
 292 Redfield ratios (Redfield et al., 1963), a strong nitrogen depletion in relation to PO_4^{3-} and Si occurred in station
 293 23. While the N:P ratio was closer to 16:1 in the rest of the stations, a general excess of PO_4^{3-} in relation to DIN
 294 was registered. On the contrary, all station except station 23, showed a Si depletion in relation to DIN. The
 295 concentration of DOC was homogeneous in the mid-shelf stations (mean of $79 \mu\text{M}$), while in the shelf break it
 296 varied from $96 \mu\text{M}$ in station 14 to $52 \mu\text{M}$ in station 13 (Fig. 2b). The highest fluorescence intensity of protein-
 297 like compounds was found in station 23, while the highest intensity of humic-like fluorophores was observed
 298 in station 21 (Fig. 3). The a_{254} was higher in the mid-shelf stations (mean of 2.3 m^{-1}) compared to the shelf
 299 break stations (mean of 1.3 m^{-1}).

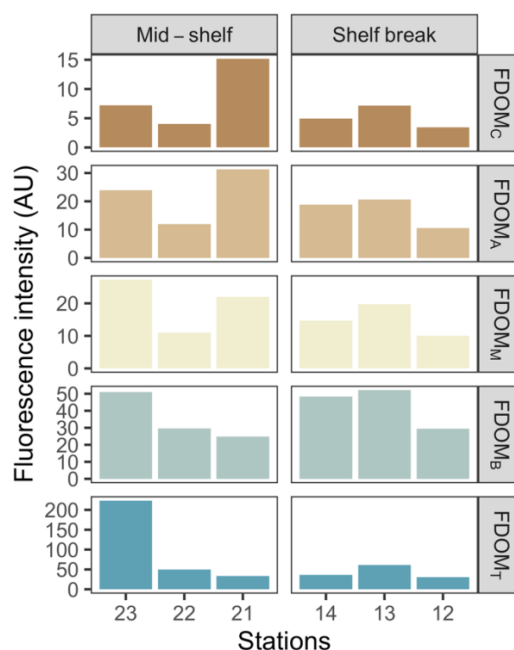
300



301

302 **Figure 2. Cumulative nutrient concentrations at the deep chlorophyll-a maximum (bars) and the**
 303 **concentration of DOC in surface waters (solid black line) across stations.**

304



305

306 **Figure 3. Fluorescence intensity of main identified FDOM components at the deep chlorophyll-a**
 307 **maximum across stations. FDOM components are shown in a decreasing order of humification from top**
 308 **to bottom plots.**

309

310 3.3 Plankton community structure

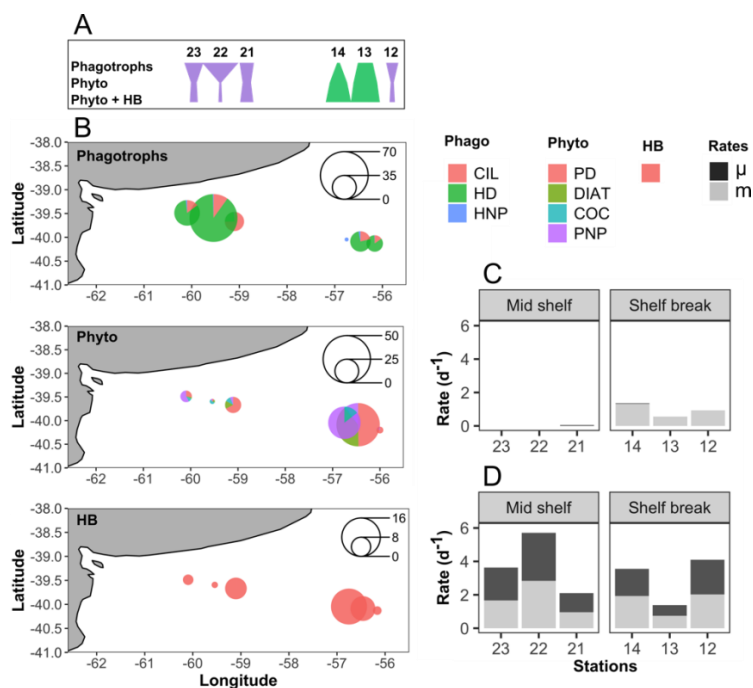
311 The type of food web structure based on the ranking of the carbon biomass of phagotrophs, phytoplankton and
 312 heterotrophic bacteria, and the spatial distribution of these groups' biomass are shown in Fig. 4a and b,
 313 respectively. Biomass of heterotrophic bacteria ranged between 2.6 (station 22) and 15 $\mu\text{g C l}^{-1}$ (station 14).

314 The abundance of this group was positively associated with chlorophyll-a concentration ($R^2=0.7$, $p=0.04$) and
 315 the abundance and biomass of most phytoplankton groups ($p<0.05$), except coccolithophores. The highest
 316 bacterial abundance and biomass was registered under chlorophyll-a pulse initiation (stations 21, 13 and 14).

317 Among phagotrophic protists, the most significant group in terms of biomass were dinoflagellates ranging from
 318 0 (station 14) to 134 $\mu\text{g C l}^{-1}$ (station 22, mostly due to the presence of *Noctiluca scintillans*). Ciliates ranged
 319 from 0 (station 14) to 20 $\mu\text{g C l}^{-1}$ (station 21), while HNP showed the highest biomass in stations 13 and 14 (5
 320 and 6 $\mu\text{g C l}^{-1}$, respectively), and the lowest value was registered in station 12 (0.6 $\mu\text{g C l}^{-1}$). Ultrazooplankton

321 (choanoflagellates and other unidentified flagellates) was the dominant fraction among HNP except in station
 322 13, were micro-sized ciliates and nano-sized flagellates (*Telonema* sp. and unidentified dinoflagellates)
 323 dominated biomass.

324



325

326

327

328

329

330

331

332

333

334

335

336

337

338

339

340

341

342

343

344

345

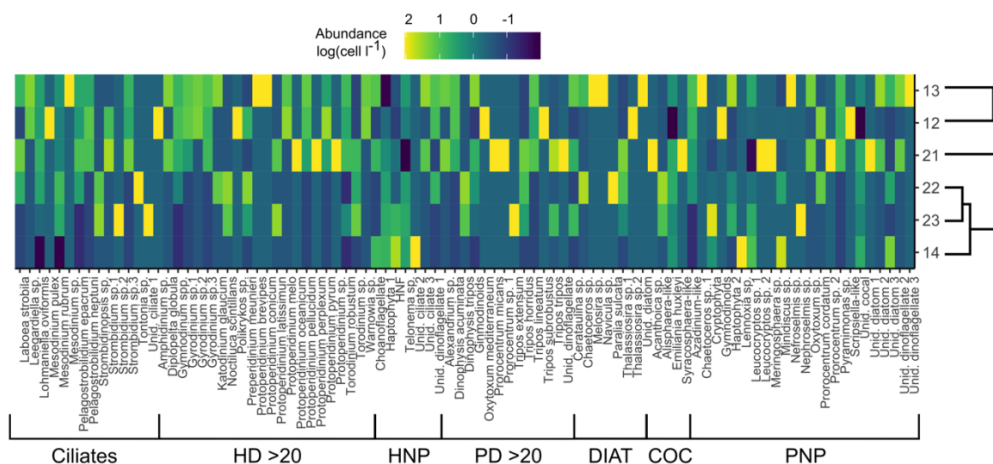
Figure 4.A. Type of food web structure based on the ranking of carbon biomass of phagotrophs, phytoplankton (phyto), and heterotrophic bacteria (HB). **B.** Spatial distribution of the cumulative biomass ($\mu\text{g C l}^{-1}$) of phagotrophs (upper plot), phytoplankton (mid-plot) and HB (lower plot). Scale circles are shown within each plot. **C.** Growth (μ) and grazing (m) rates of phytoplankton. **D.** Growth (μ) and grazing (m) rates of HB.

Whitin phytoplankton, four main groups were identified: photosynthetic nanoplankton (PNP, including photosynthetic nanoflagellates, nano-sized diatoms and dinoflagellates), micro-sized photosynthetic dinoflagellates (PD), micro-sized diatoms, and coccolithophores. PNP generally dominated the biomass of photosynthetic taxa. The highest concentration and biomass of all groups, except for coccolithophores, was registered in station 13 (PNF: $32 \mu\text{g C l}^{-1}$, PD: $8 \mu\text{g C l}^{-1}$, diatoms: $6 \mu\text{g C l}^{-1}$). High biomass of PNP and dinoflagellates was also registered in station 14 ($34 \mu\text{g C l}^{-1}$) and station 21 ($8.5 \mu\text{g C l}^{-1}$), respectively. The highest biomass of coccolithophores was registered in station 22 ($2 \mu\text{g C l}^{-1}$).

Stations 12 and 13 showed conspicuous differences on microplankton community structure compared to the rest of the stations (Fig. 5). According to the ordination fit between vectors (i.e., taxa) and stations, the phagotrophic species that mainly contributed to separate these two stations from the others were the dinoflagellates *Gymnodinium* spp., and *Protoperidinium pellucidum*, while *Pyramimonas* sp. and *Dinophysis acuminata*, were the distinctive photosynthetic species in these stations (MDS, $p < 0.05$). Stations 22 and 23 were also closely associated regarding the heterotrophic community and the species that contributed most to this association was *Strombidinopsis* sp.



346



347

348

349

350

351

352

353

354

355

3.4 Growth and grazing rates

356

357

358

359

360

361

362

363

364

365

366

367

368

369

Figure 5. Color-coded, log-transformed cell abundance ($\text{cell l}^{-1} \times 10^3$) of plankton taxa (columns) at the sampling stations (rows). Functional groups delimitation is indicated in the bottom. Side dendrogram shows the optimal ordering of rows (stations) so that the sum of distances between each one is minimized. HD>20: Heterotrophic dinoflagellates >20 μm , HNP: Heterotrophic nanoplankton, PD>20: Photosynthetic dinoflagellates >20 μm , Diat: Diatoms, Coc: Coccolithophores, PNP: Photosynthetic nanoplankton.

Water temperature of the incubator container was hourly monitored and ranged between 12.2 and 13.8°C in the mid-shelf stations and between 8 and 11.1°C in the shelf break stations. Bacteria showed active growth during all experiments while phytoplankton only revealed significant growth rates in conditions of pulse initiation (stations 21 and 14). Some degree of nutrient limitation was detected in the mid-shelf stations as the growth rate of phytoplankton at the control treatments was lower than in the nutrient amended treatment, however, differences were not statistically significant. No apparent differences were found in stations 12,13 and 14. Significant grazing effect on bacteria was found in all experiments (Fig. 4c), while grazing on phytoplankton was only significant in the shelf break stations (Fig. 4d). In the mid-shelf stations, daily bacterial productivity consumed by HNP averaged 72%, while in the shelf break stations, it reached 83%. Mean daily primary productivity consumed by phagotrophic protists was zero in the mid-shelf stations and 155% in the shelf break. Linear responses were found in all experiments, indicating that no cascading effects, saturating feeding and or starvation occurred within incubation bottles. The abundance of heterotrophic bacteria was negatively correlated with the grazing of HNP ($R^2=0.8$, $p=0.016$) and growth ($R^2=0.9$, $p=0.005$).

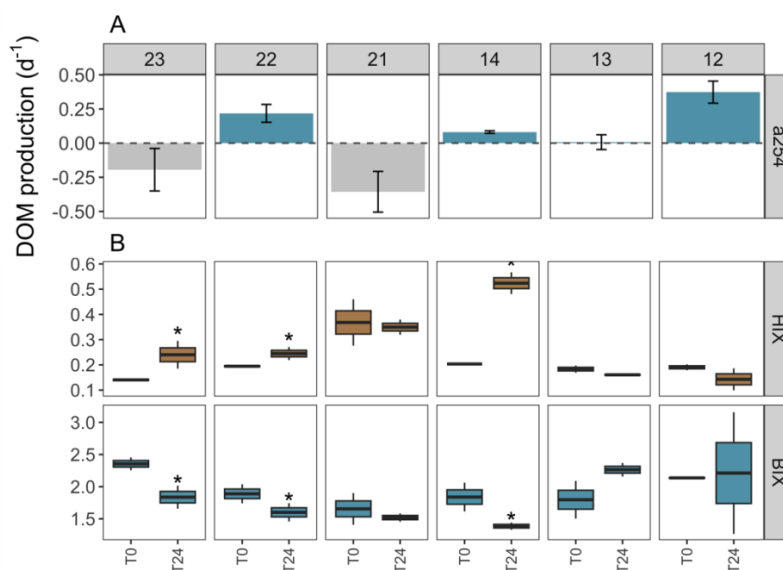


370 **3.5 Short-term DOM transformations**

371 DOM accumulation was observed in stations 22, 14, 13, and 12 during the incubation period in the experimental
 372 setting with protists, while stations 23 and 21 exhibited DOM consumption (Fig. 6a). Conversely, in the
 373 experimental setting without protists, DOM accumulated in stations 22, 21, 14, and 12, while stations 23 and
 374 13 showed DOM consumption (Fig. 7a). Regardless of net DOM production, biodegradation of organic matter
 375 occurred in most experiments as denoted by the decrease of the BIX and the increase on the HIX (Fig. 6b, 7b).
 376 The prevalence of biodegradation over UV photodegradation or adsorption was further supported by most
 377 source discrimination indices (FI and M/A, data not shown). The decrease on BIX was coherent with the net
 378 zero to low phytoplankton growth during our experiments. An exception to this general pattern occurred in
 379 station 13, in which HIX increased and BIX decreased during the incubation. Station 13 was characterized by
 380 the highest abundance of micro-sized phytoplankton (diatoms and photosynthetic dinoflagellates) and
 381 registered the lowest concentration of DOC (52 μM) at the moment of sampling. While HIX and BIX indices
 382 suggested that DOM modifications are not driven by biodegradation, M/A decreased and FI increased during
 383 the experiments, thus giving inconsistent results.

384 Among treatments, a shift from DOM accumulation to consumption was registered in stations 21 and 13. In the
 385 presence of protists, the net DOM production was negatively associated with the fluorescence intensity of peaks
 386 related to humic-like compounds (FDOM_C : $R^2=0.6$, $p=0.07$, FDOM_A , $R^2=0.8$, $p=0.01$, FDOM_M : $R^2=0.7$,
 387 $p=0.04$), and positively associated with the grazing on HB ($R^2=0.7$, $p=0.00$). In the absence of protists, the net
 388 DOM production was negatively associated with the ratio between bacteria and phytoplankton biomass ($R^2=0.9$,
 389 $p=0.01$) (Fig. 8).

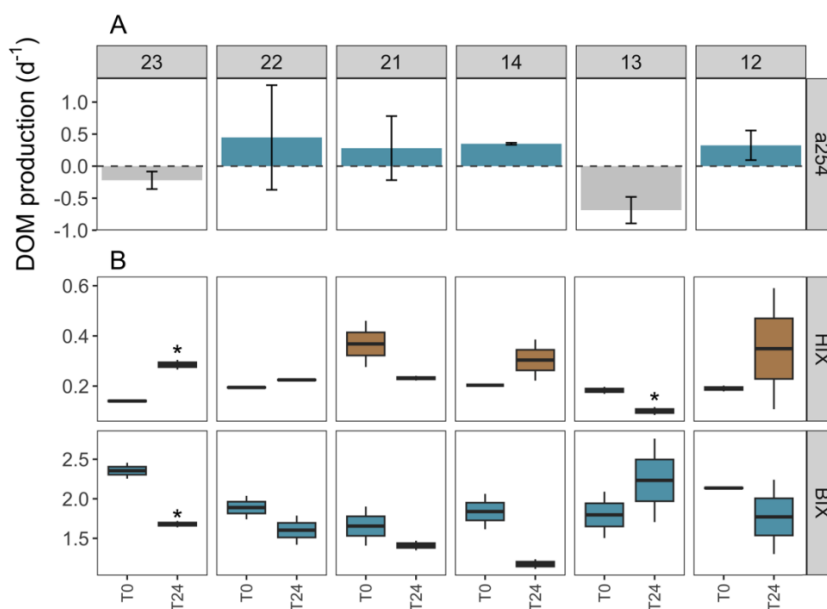
390



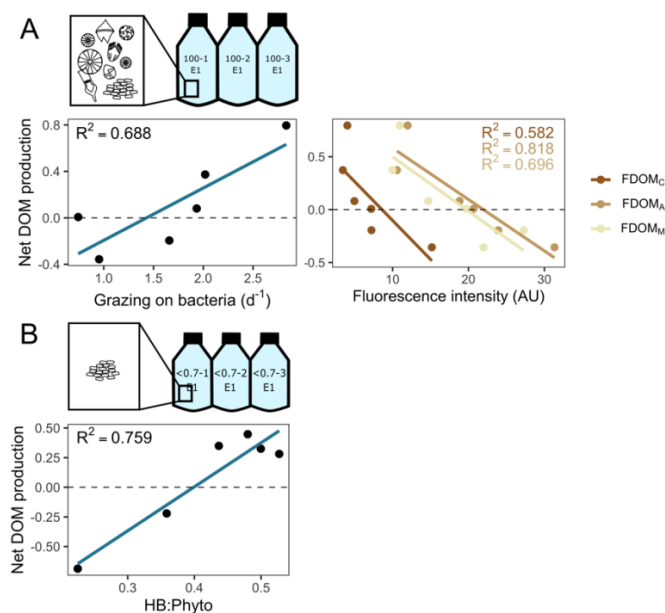
391



392 **Figure 6. DOM transformations in the experimental setting with protists (prefiltered by 200 μm) across**
 393 **stations. A. Net DOM production as depicted by the absorbance intensity at 254 nm, a proxy of total**
 394 **DOM concentration. Dashed line indicates the limit between net DOM consumption (negative values)**
 395 **and net DOM accumulation (positive values). B. Shifts in the humification index (HIX) and the biological**
 396 **activity index (BIX) during the 24-h incubation. Asterisks indicate significant differences identified by**
 397 **linear regression analysis between initial and final treatments ($p < 0.05$).**
 398



399 **Figure 7. DOM transformations in the experimental setting without protists (prefiltered by 0.7 μm)**
 400 **across stations. A. Net DOM production as depicted by the absorbance intensity at 254 nm, a proxy of**
 401 **total DOM concentration. Dashed line indicates the limit between net DOM consumption (negative**
 402 **values) and net DOM accumulation (positive values). B. Shift in the humification index (HIX) and the**
 403 **biological activity index (BIX) during the 24-h incubation. Asterisks indicate significant differences**
 404 **identified by linear regression analysis between initial and final treatments ($p < 0.05$).**
 405
 406



407

408 **Figure 8. Main predictors of the net dissolved organic matter (DOM) production during incubations. A.**
 409 **Experimental setting with protists. Linear regression plots depict the relationship between net DOM**
 410 **production and grazing on bacteria, and humic-like substances (as depicted by fluorophores FDOM_C,**
 411 **FDOM_A, and FDOM_M). B. Experimental setting without protists. Linear regression plot depicts the**
 412 **relationship between net DOM production and the ratio between heterotrophic bacteria (HB) and**
 413 **phytoplankton (Phyto) biomass. Dashed lines indicate the limit between net DOM consumption (negative**
 414 **values) and net DOM accumulation (positive values).**

415

416 **4 Discussion**

417 **4.1 Microbial food web structure**

418 The composition and distribution of the plankton community varied notably between blooming and non-
 419 blooming stations across our study area. Station 14 separated from this ordination due to its unique plankton
 420 structure resembling non-blooming areas, despite its location within a blooming region. This anomaly may be
 421 attributed to the dominance of a single nanoplanktonic diatom species, which accounted for a significant portion
 422 of the photosynthetic biomass, alongside a predominantly ultra and nano-sized protistan grazer community.
 423 Moreover, station 14 exhibited the highest bacterial biomass, suggesting a prevalence of small planktonic
 424 organisms favored by resource stoichiometry characterized by low PO₄³⁻ and Si concentrations but high surface
 425 DOC. Furthermore, the location of station 14, coastward of the 100 m isobath and outside the Malvinas Current
 426 jets, indicates that nutrient-rich upwelling events at this site may be intermittent (Franco et al., 2008).

427 The analysis of biomass distribution among photosynthetic plankton revealed the predominance of ultra- and
 428 nanophytoplankton, with solitary diatoms, cryptophytes, haptophytes, and *Azadinium*-like dinoflagellates being



429 the most notable representatives within these size classes. Similar findings were reported in previous studies by
430 Negri et al. (2013, 2016) and Silva et al. (2009), indicating the widespread dominance of ultraphytoplankton,
431 primarily *Synechococcus*, in the region. Although cyanobacteria were not quantified in our study, they are
432 assumed to play a crucial role in carbon fixation and immobilization, particularly during warm months. In the
433 shelf break area, nano-sized phytoplankton, particularly diatoms, were dominant, as reported by Carreto et al.
434 (2016). Micro-sized phytoplankton biomass was mostly comprised of photosynthetic dinoflagellates, followed
435 closely by diatoms, consistent with findings by Ferronato et al. (2021, 2023), in the mid-shelf and shelf break
436 areas during spring conditions.

437 Dinoflagellates also dominated the biomass of phagotrophic protists, with *Noctiluca scintillans* and nano-sized
438 dinoflagellates being the primary contributors, as observed by (Carreto et al., 2016) in the shelf break area.
439 Ciliates, particularly nano-sized taxa, were the second most important contributors to heterotrophic biomass,
440 followed by micro-sized ciliates such as *Laboea strobila*. No clear distribution patterns in protistan grazers were
441 observed, a phenomenon well-documented in marine habitats associated with factors such as compositional
442 turnover, dispersal ability, differential environmental response, and interspecific interactions, coupled with
443 local bloom timing (Grattepanche et al., 2016; Péquin et al., 2022; Snyder et al., 2021; Zhao et al., 2022).
444 Mesoscale and submesoscale structures in the Patagonian Shelf create spatial heterogeneity, impacting the
445 distribution of dissolved resources (Garzón-Cardona et al., 2021) and chlorophyll-a (Becker et al., 2023;
446 Saraceno et al., 2024). The stirring produced by these processes, while understudied at the local scale, is
447 fundamental in driving the three-dimensional distribution of plankton (Lehahn et al., 2018). Furthermore, the
448 mosaic distribution of nutrients in turbulent areas may alter bacterial composition, with different nutrient
449 affinities potentially reshaping the entire microbial interactome (Delgadillo-Nuño et al., 2024).

450 The abundance and biomass of heterotrophic bacteria fell within the reported minimum values for spring and
451 summer in the study area, particularly resembling values typically observed during summer in the coastal zone
452 (<50 m depth) (Garzón-Cardona et al., 2021; Hozbor et al., 2013; Negri et al., 2016). While prior studies in this
453 sector did not establish a clear link between heterotrophic bacterial abundance and chlorophyll-a, it is commonly
454 noted that bacteria thrive in frontal regions with high phytoplankton concentrations and secondary production.
455 In addition, previous research has indicated a positive correlation between bacterial abundance and dissolved
456 organic carbon (Garzón-Cardona et al., 2021). In our study, we did not observe significant relationships between
457 bacteria and DOM proxies (i.e., a₂₅₄), while we did find a significant positive relationship with chlorophyll-a.
458 In turn, bacterial abundance exhibited a negative response to high HNP grazing pressure. This suggests that
459 during periods of high productivity in spring, bacterial distribution is influenced not only by the supply of fresh
460 DOM from phytoplankton but also by grazing-induced mortality. The intermittent coupling between bacteria
461 and phytoplankton and the lack of reported relationships between bacteria and inorganic nutrients also suggest
462 that bacteria are weakly resource-controlled in this area. Instead, considering that the control of grazing on
463 bacterial biomass is more pronounced under conditions of low bottom-up regulation (Morán et al., 2017), our
464 results suggest that under the examined conditions bacteria are top-down controlled, with maximum attainable
465 biomass limited by grazing pressure as well as other unidentified sources of mortality.

466



467 **4.2 Microbial trophic pathways**

468 Our findings are in line with previous observations in the region, emphasizing the tight trophic coupling and
469 minimal sinking of unused prey biomass (Negri et al., 2013). This is attributed to the spatial uniformity of the
470 trophic network composition, characterized by the dominance of small phytoplankton (<5 μm) and micro- and
471 mesozooplankton groups, which exhibit comparable biomass magnitudes. Indeed, group-specific biomass
472 distribution of <200 μm plankton in this study, revealed that except for station 13 and 14 that were at the bloom
473 peak, mid-shelf stations and station 12 (post-bloom) showed a top-heavy biomass distribution or inverted
474 pyramid. Drivers of top-heaviness are linked to high trophic transfer efficiency, faster turnover of prey than
475 consumers, or omnivory that bypasses inefficient trophic levels (McCauley et al., 2018). Since the turnover of
476 phytoplankton and bacteria is similar to that of protistan grazers, the most likely reason for the inverted pyramid
477 structure is a high trophic efficiency and the presence of omnivore consumers. Protists are known to be highly
478 efficient feeders (Weisse et al., 2016), particularly under high prey abundance, and trophic transfer is
479 significantly increased by the presence of mixotrophs (Ward and Follows, 2016). Although mixotrophy was not
480 directly assessed in this study, the predominance of nanoflagellates among protistan grazers implies a potential
481 significant role of mixotrophy in shaping the trophic structure of the microbial community (Edwards, 2019). In
482 contrast, the classical bottom-heavy pyramid biomass structure of plankton was registered under bloom peak at
483 shelf break stations 13 and 14. Despite intense predation on phytoplankton in the shelf break stations, the
484 biomass accumulation resulting from a higher carrying capacity, driven by local upwelling, was sufficient to
485 maintain the typical biomass pyramid structure, with photosynthetic taxa dominating plankton biomass. This
486 type of food web structure attains the highest carbon biomass regardless of community composition (Kang et
487 al., 2023), and suggests that under productive conditions within the upwelling front, a fraction of primary
488 production escapes predation by protists and is either exploited by microcrustaceans or advected by mixing or
489 sinking processes.

490 Our results denoted active growth of heterotrophic bacteria in all stations, while phytoplankton evidenced low
491 net growth or biomass yield. Low growth rate of phytoplankton was only detected in station 21 at the bloom
492 initiation and in station 14 at the last stage of the ascending bloom ramp. Despite possessing half the biomass
493 of phytoplankton, grazers selectively preyed upon heterotrophic bacteria and accounted for 72% of bacterial
494 production in the mid-shelf stations while phytoplankton production was not significantly affected by grazing.
495 This selective grazing on bacteria can likely be attributed to their higher growth rate compared to that of
496 phytoplankton, as protistan grazing is known to be activated in response to changes in prey availability (Banse,
497 1982; Chen et al., 2009). In fact, grazing by HNP showed a negative relationship with bacterial biomass,
498 denoting that prey growth is a better activator than their biomass. Consequently, bacteria exhibited growth
499 advantages over phytoplankton across the examined environmental gradient but were concurrently more
500 vulnerable to grazing pressure. This compensatory grazing on fast-growing bacteria has been previously
501 observed in productive environments such as the California Current (Goericke, 2011; Landry et al., 2023;
502 Taylor and Landry, 2018a) as well as in the oligotrophic Warm Taiwan Current (Chiang et al., 2014). The
503 suggested mechanism underlying this trophic interaction posits that increased phytoplankton-DOM production
504 fosters the growth of resource-efficient bacteria as suggested by the tight coupling between bacteria and



505 phytoplankton biomass. However, the heightened growth, coupled with a diminished allocation of energy to
506 defensive skills, renders these bacteria susceptible to selective grazing (Taylor and Landry, 2018a).

507 The situation in the more productive shelf break area, shifted toward a coupled predation upon both prokaryotes
508 and phytoplankton (Fig. 9a). Grazing accounted for 83% of bacterial production and 154% of phytoplankton
509 production. Despite limited growth, phytoplankton faced substantial grazing pressure, possibly facilitated by
510 shared predators with bacteria. This trophic interaction aligns with the enhanced microbial loop hypothesis
511 (Taylor and Landry, 2018b), suggesting that small phytoplankton is increasingly grazed as a byproduct of
512 grazers actively preying on bacteria under conditions of rising productivity. Under this scenario, grazing on
513 picophytoplankton is density-independent and occurs due to the presence of shared common grazers with
514 bacteria. Across stations, density-dependent control mechanisms further regulated the standing stock of
515 bacteria, with mechanisms reducing population density likely conferring benefits by preventing rapid resource
516 depletion. Overall, bacteria appeared to be positively regulated by commensalism with phytoplankton and
517 negatively by grazing, constituting a primary carbon source for protistan grazers regardless of the productivity
518 level.

519

520 **4.3 Short-term DOM pathways**

521 A general trend denoting weak DOM limitation of bacterial growth was found, as even in the experiments
522 without DOM-producing phytoplankton, organic matter accumulated in most experiments. During the
523 experiments, high bacterial growth, and net zero or low phytoplankton growth coincided with active
524 biodegradation of organic matter, as indicated by the decline in the biological index (BIX) and the rise in the
525 humification index (HIX). The general decreasing trend of BIX during the incubation and its similar behaviour
526 in the absence of protist confirms a bacterial effect and suggest that bacteria are rapidly consuming recently
527 produced phytoplankton exudates. Similar observations have shown bacterial production of humic-like
528 substances from protistan plankton precursors under experimental conditions devoid of terrestrial influence
529 (Gruber et al., 2006; Kinsey et al., 2018; Lechtenfeld et al., 2015; Osburn et al., 2019; Romera-Castillo et al.,
530 2011), underscoring the significance of microbial communities in immobilizing DOM in the form of refractory
531 substances over short timescales. The findings of this study enhance our understanding of the mechanisms
532 underlying the Patagonian Shelf's role as a hotspot for carbon sequestration (Kahl et al., 2017). The described
533 carbon route partially explains why the region acts as a carbon sink throughout most of the year, irrespective of
534 the primary productivity magnitude. These results underscore the critical role of the microbial carbon pump
535 (Jiao et al., 2024) as a key carbon sequestration pathway within non-frontal areas of the Patagonian Shelf. While
536 these findings highlight its importance, the seasonal relevance of this mechanism remains to be explored.

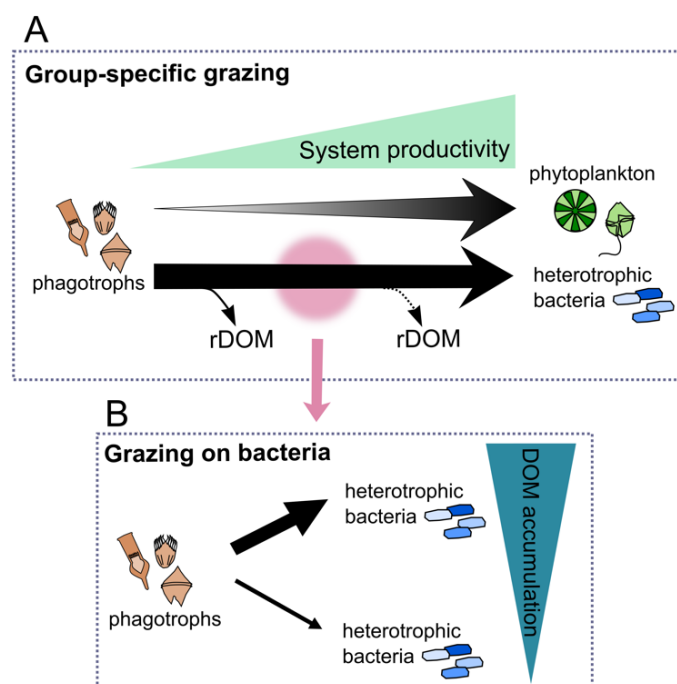
537 The accumulation of DOM was not limited to stations experiencing active phytoplankton growth, indicating
538 that net DOM release is not necessarily tied to specific phenological stages, as previously suggested (Bachi et
539 al., 2023). Moreover, it was not correlated with phytoplankton species composition, implying a low level of
540 specialization in the bacterial utilization of species-specific DOM substances, a trait that becomes apparent
541 under conditions of high resource availability (Sarmiento et al., 2016). Instead, the degree of complexity of
542 DOM expressed as the prevalence of humic compounds (F_{DOMC}, F_{DOMA}, and F_{DOMM}), emerged as a



543 primary factor determining its utilization by bacteria. Detectable consumption occurred when the initial DOM
544 pool presented a high contribution of low reactivity compounds, likely resulting from the phenological status
545 of the sampling point as depicted by the temporal progression of satellite chlorophyll-a. This scenario was
546 observed at stations 23 and 21, where sampling was preceded by low chlorophyll-a content, indicating limited
547 autochthonous production of fresh DOM in the preceding month. However, the differences in bacterial growth
548 and FDOM-inferred biodegradation at both stations suggest variations in bacterial activity. At station 23, intense
549 bacterial activity was evidenced by the significant increase in the complexity of DOM and the net DOM
550 consumption under both treatments. Despite the high contribution of refractory compounds in this site (FDOM_C,
551 FDOM_A, and FDOM_M), the initial labile DOM pool was also high (particularly FDOM_T), denoting that bacteria
552 may have sustained their growth upon this labile initial stock over the 24 h incubation under the absence of
553 DOM-producing phytoplankton. Interestingly, under the absence of protists, DOM consumption shifted to
554 accumulation in station 21. At this station, a notable abundance of initial refractory compounds was observed.
555 In contrast to observations at station 23, bacterial activity was low, as indicated by a low growth rate and no
556 detectable biodegradation of DOM. Therefore, the apparent decrease of bacterial DOM utilization under the
557 absence of protists, suggests that bacterial reliance on phytoplankton DOM exudates increases when the existing
558 DOM pool consists primarily of refractory compounds. Despite similar phenological stage, this situation was
559 not observed in station 22, where the degree on refractory compound was lower. This suggests the presence of
560 other sources of labile DOM that may not be adequately represented by total chlorophyll-a measurements, such
561 as *Synechococcus*, a significant picophytoplankton genus in the shelf area (Silva et al., 2009) known to
562 contribute to bioavailable DOM production (Zheng et al., 2019).

563 The opposite scenario, i.e., a shift from weak DOM accumulation to DOM consumption under the absence of
564 protists, was observed in station 13. Here, the initial proportion of labile DOM was higher, denoting that DOM
565 bioavailability did not restrict bacterial activity. This station displayed the lowest biomass ratio between
566 phytoplankton and bacteria, indicating that DOM consumption in the absence of protists occurred when the
567 initial phytoplankton biomass significantly surpassed that of heterotrophic bacteria. This suggests that the initial
568 phytoplankton biomass masked intense bacterial DOM utilization, which only became evident upon the removal
569 of protists. However, DOM accumulation might be overestimated due to the input of DOM lysates resulting
570 from viral lysis. Indeed, the decrease in HIX alongside the increase in BIX observed in station 13 under both
571 treatments suggests that viruses are transferring bacterial biomass into the labile DOM pool (Proctor and
572 Fuhrman, 1991). The low bacterial growth and grazing at this site along with the station's bloom timing further
573 support this notion, as it suggests that sampling occurred at the transition between grazing control to viral
574 control of bacterial biomass. Indeed, the latter tends to occur under low grazing pressure (Bettarel et al., 2004;
575 Pasulka et al., 2015). Overall, the fact that DOM accumulation occurred even in the absence of protists, indicates
576 that bacteria are the main source of DOM as previously noted (Gruber et al., 2006). The initial proportion of
577 refractory compounds better predicted the net DOM production by providing insights on microbial succession
578 trajectories.

579



580

581 **Figure 9. Grazing-mediated pathways of DOM in the Patagonian Shelf. A. While phytoplankton biomass**
 582 **was found to be twice that of bacteria, a selective grazing on bacteria was observe compensating for their**
 583 **fast growth rate along the productivity gradient. In turn, grazing on phytoplankton increased with rising**
 584 **productivity, suggesting that phytoplankton, particularly smaller cells, are increasingly grazed as a**
 585 **byproduct of intense grazing on bacteria, aligning with the enhanced microbial loop hypothesis.**
 586 **Heterotrophic bacteria were the primary agents shaping DOM quality, capable of storing carbon in the**
 587 **refractory DOM pool (rDOM) even in the absence of DOM-producing protists. However, the production**
 588 **of rDOM was more conspicuous in mid-shelf stations than in the shelf break. B. Grazing on bacteria**
 589 **influenced the net production of DOM. Arrows thickness represents grazing pressure. Pronounced**
 590 **bacterial grazing led to an accumulation of DOM, likely by reducing the biomass of bacterial standing**
 591 **stock and by contributing with egestion organic substances.**

592

593 DOM also tended to accumulate under high bacterial mortality due to grazing. Our results evidenced that carbon
 594 was primarily channeled from prokaryotes to protistan grazers, bypassing slower growing phytoplankton. This
 595 group-specific grazing mortality align well with the grazing selectivity model, wherein grazers exhibit
 596 preferences against high-growth-rate organisms, establishing a tight coupling between growth advantages and
 597 grazing vulnerability across environmental gradients (Landry et al., 2023). Our experimental data not only
 598 support this hypothesis but also provide new insights into the repercussions of bacterial grazing on dissolved
 599 carbon stocks (Fig. 9b). Specifically, our results suggest that grazing on bacteria can lead to an accumulation
 600 of DOM produced by phytoplankton by reducing the biomass of bacterial standing stock. In addition, protistan



601 grazing may contribute to the DOM pool by releasing bacterial carbon (Taylor et al., 1985). However, bacteria
602 may not immediately utilize this DOM source, as adapting their enzymatic machinery to target new compounds
603 requires additional energy expenditure, resulting in less efficient resource utilization (Baña et al., 2014). Similar
604 results were observed in polar waters, where high protistan bacterivory was associated with DOM accumulation
605 (Lund Paulsen et al., 2019). Our observations carry biogeochemical implications, as intense bacterial grazing
606 implies that bacterial biomass becomes available to higher trophic levels, thereby circumventing the DOM
607 cycle. In other words, while most bacterial biomass is directed by protistan grazers toward higher trophic levels,
608 it also partially diverts the production of DOM lysates by viral lysis (Suttle, 2005). Our experimental results
609 also indicate that intense grazing only partially compensates for this carbon route, as a fraction of
610 phytoplankton-derived DOM remains unexploited by bacteria over short timescales.

611 The fate of grazing-derived DOM remains uncertain in our experimental setup, as it could either serve as a
612 potential source for bacterial utilization, thus establishing a positive longer-term predator-prey feedback not
613 captured in our 24-h experiment, or contribute to the complex DOM pool, feeding into the refractory fraction.
614 Indeed, previous observations revealed that DOM derived from protistan grazers varies in its bioavailability
615 (Taylor et al., 1985), and their complexity is further shaped by taxa composition (Gruber et al., 2006; Nagata
616 and Kirchman, 1992). In our experiments, we did not observe a clear trend in DOM transformation between
617 treatments with and without protists, indicating that bacteria remain as the primary shapers of DOM quality.
618 Overall, our finding revealed that under high bacterial growth rate that follows the onset of the productive
619 season, protistan grazers not only channels carbon through remineralization but also, foster the degree of DOM
620 accumulation by reducing DOM-degrading bacterial stock and contributing with egestion substances.
621 Additionally, instead of acting solely as a sink of carbon through mineralization of organic compound, bacteria
622 serve as a crucial link between assimilatory CO₂ and higher trophic levels.

623

624 **Data availability**

625 DOI: 10.5281/zenodo.11662261

626

627 **Authors contribution**

628 CLA conceptualized, designed, and carried out the experiments, analyzed plankton samples and acquired
629 funding. JEGC, AM and ASG analyzed DOC, CDOM, FDOM and nutrients samples and interpreted the results.
630 JEGC performed the PARAFAC multivariate algorithm and calculated fluorescence indices. RS analyzed
631 plankton samples and performed biomass calculations. JCM contributed to the numerical methodology design
632 and the conceptualization of overarching goals. LARE analyzed and interpreted CTD data and Moderate
633 Resolution Imaging Spectroradiometer (MODIS) Aqua images of chlorophyll-a. RL coordinated
634 responsibilities for the research activities planning and execution, acquired funding and contributed to the
635 conceptualization of overarching goals. CLA prepared the manuscript with contributions from all co-authors.

636



637 **Competing interests**

638 The authors declare no competing interests.

639

640 **Acknowledgments**

641 We are thankful to the crew of the RV “Dr. Bernardo Houssay” of Prefectura Naval Argentina for their support
642 on field activities and sampling. This study was supported by the National Agency for Promotion of Science
643 and Technology (FONCYT-PICT 0467–2010 and FONCYT-PICT 2386-2017), the National Scientific and
644 Technical Research Council (CONICET-PIP 11220200102681CO) and by the Argentine Oceanographic
645 Institute (IADO, CONICET-UNS). The authors acknowledge that language checking and spelling
646 improvements were done by ChatGPT (powered by OpenAI's language model, GPT-3; <http://openai.com>).

647

648 **References**

- 649 Azam, F., Fenchel, T., Field, J., Gray, J., Meyer-Reil, L., and Thingstad, F.: The Ecological Role of Water-
650 Column Microbes in the Sea, *Mar Ecol Prog Ser*, 10, 257–263, <https://doi.org/10.3354/meps010257>, 1983.
- 651 Bachi, G., Morelli, E., Gonnelli, M., Balestra, C., Casotti, R., Evangelista, V., Repeta, D. J., and Santinelli,
652 C.: Fluorescent properties of marine phytoplankton exudates and lability to marine heterotrophic prokaryotes
653 degradation, *Limnol Oceanogr*, 68, <https://doi.org/10.1002/lno.12325>, 2023.
- 654 Bai, Y., Su, R., Han, X., Zhang, C., and Shi, X.: Investigation of seasonal variability of CDOM fluorescence
655 in the southern changjiang river estuary by EEM-PARAFAC, *Acta Oceanologica Sinica*, 34, 1–12,
656 <https://doi.org/10.1007/s13131-015-0714-8>, 2015.
- 657 Baltar, F., Palovaara, J., Unrein, F., Catala, P., Horňák, K., Šimek, K., Vaqué, D., Massana, R., Gasol, J. M.,
658 and Pinhassi, J.: Marine bacterial community structure resilience to changes in protist predation under
659 phytoplankton bloom conditions, *ISME J*, 10, 568–581, <https://doi.org/10.1038/ismej.2015.135>, 2016.
- 660 Baña, Z., Ayo, B., Marrasé, C., Gasol, J. M., and Iriberrí, J.: Changes in bacterial metabolism as a response to
661 dissolved organic matter modification during protozoan grazing in coastal Cantabrian and Mediterranean
662 waters, *Environ Microbiol*, 16, 498–511, <https://doi.org/10.1111/1462-2920.12274>, 2014.
- 663 Banse, K.: Cell volumes, maximal growth rates of unicellular algae and ciliates, and the role of ciliates in the
664 marine pelagial1,2, *Limnol Oceanogr*, 27, 1059–1071, <https://doi.org/10.4319/lo.1982.27.6.1059>, 1982.
- 665 Becker, F., Romero, S. I., and Pisoni, J. P.: Detection and characterization of submesoscale eddies from
666 optical images: a case study in the Argentine continental shelf, *Int J Remote Sens*, 44, 3146–3159,
667 <https://doi.org/10.1080/01431161.2023.2216853>, 2023.
- 668 Berden, G., Charo, M., Möller, O. O., and Piola, A. R.: Circulation and Hydrography in the Western South
669 Atlantic Shelf and Export to the Deep Adjacent Ocean: 30°S to 40°S, *J Geophys Res Oceans*, 125,
670 <https://doi.org/10.1029/2020JC016500>, 2020.
- 671 Berglund, J., Müren, U., Båmstedt, U., and Andersson, A.: Efficiency of a phytoplankton-based and a
672 bacterial-based food web in a pelagic marine system, *Limnol Oceanogr*, 52, 121–131,
673 <https://doi.org/10.4319/lo.2007.52.1.0121>, 2007.



- 674 Bettarel, Y., Sime-Ngando, T., Amblard, C., and Dolan, J.: Viral Activity in Two Contrasting Lake
675 Ecosystems, *Appl Environ Microbiol*, 70, 2941–2951, <https://doi.org/10.1128/AEM.70.5.2941-2951.2004>,
676 2004.
- 677 Brandstetter, A., Sletten, R. S., Mentler, A., and Wenzel, W. W.: Estimating dissolved organic carbon in
678 natural waters by UV absorbance (254 nm), *Zeitschrift für Pflanzenernährung und Bodenkunde*, 159, 605–
679 607, <https://doi.org/10.1002/jpln.1996.3581590612>, 1996.
- 680 Brussaard, C. P. D.: Viral Control of Phytoplankton Populations—a Review, *Journal of Eukaryotic*
681 *Microbiology*, 51, 125–138, <https://doi.org/10.1111/j.1550-7408.2004.tb00537.x>, 2004.
- 682 Calbet, A. and Landry, M. R.: Phytoplankton growth, microzooplankton grazing, and carbon cycling in
683 marine systems, *Methods*, 49, 51–57, 2004.
- 684 Calbet, A. and Saiz, E.: How much is enough for nutrients in microzooplankton dilution grazing
685 experiments?, *J Plankton Res*, 40, 109–117, <https://doi.org/10.1093/plankt/fbx070>, 2018.
- 686 Carreto, J. I., Montoya, N. G., Carignan, M. O., Akselman, R., Acha, E. M., and Derisio, C.: Environmental
687 and biological factors controlling the spring phytoplankton bloom at the Patagonian shelf-break front –
688 Degraded fucoxanthin pigments and the importance of microzooplankton grazing, *Prog Oceanogr*, 146, 1–21,
689 <https://doi.org/10.1016/j.pocean.2016.05.002>, 2016.
- 690 Cavicchioli, R., Ripple, W. J., Timmis, K. N., Azam, F., Bakken, L. R., Baylis, M., Behrenfeld, M. J.,
691 Boetius, A., Boyd, P. W., Classen, A. T., Crowther, T. W., Danovaro, R., Foreman, C. M., Huisman, J.,
692 Hutchins, D. A., Jansson, J. K., Karl, D. M., Koskella, B., Mark Welch, D. B., Martiny, J. B. H., Moran, M.
693 A., Orphan, V. J., Reay, D. S., Remais, J. V., Rich, V. I., Singh, B. K., Stein, L. Y., Stewart, F. J., Sullivan,
694 M. B., van Oppen, M. J. H., Weaver, S. C., Webb, E. A., and Webster, N. S.: Scientists’ warning to humanity:
695 microorganisms and climate change, *Nat Rev Microbiol*, 17, 569–586, <https://doi.org/10.1038/s41579-019-0222-5>, 2019.
- 697 Chen, B., Liu, H., Landry, M. R., DaI, M., Huang, B., and Sune, J.: Close coupling between phytoplankton
698 growth and microzooplankton grazing in the western South China Sea, *Limnol Oceanogr*, 54, 1084–1097,
699 <https://doi.org/10.4319/lo.2009.54.4.1084>, 2009.
- 700 Chiang, K.-P., Tsai, A.-Y., Tsai, P.-J., Gong, G.-C., Huang, B.-Q., and Tsai, S.-F.: The influence of
701 nanoflagellates on the spatial variety of picoplankton and the carbon flow of the microbial food web in the
702 oligotrophic subtropical pelagic continental shelf ecosystem, *Cont Shelf Res*, 80, 57–66,
703 <https://doi.org/10.1016/j.csr.2014.02.019>, 2014.
- 704 Coble, P. G.: Characterization of marine and terrestrial DOM in seawater using excitation-emission matrix
705 spectroscopy, *Mar Chem*, 51, 325–346, [https://doi.org/10.1016/0304-4203\(95\)00062-3](https://doi.org/10.1016/0304-4203(95)00062-3), 1996.
- 706 Delgadoillo-Nuño, E., Teira, E., Pontiller, B., Lundin, D., Joglar, V., Pedrós-Alió, C., Fernández, E., Pinhassi,
707 J., and Martínez-García, S.: Coastal upwelling systems as dynamic mosaics of bacterioplankton functional
708 specialization, *Front Mar Sci*, 10, <https://doi.org/10.3389/fmars.2023.1259783>, 2024.
- 709 Delgado, A. L., Hernández-Carrasco, I., Combes, V., Font-Muñoz, J., Pratalongo, P. D., and Basterretxea, G.:
710 Patterns and Trends in Chlorophyll-a Concentration and Phytoplankton Phenology in the Biogeographical
711 Regions of Southwestern Atlantic, *J Geophys Res Oceans*, 128, <https://doi.org/10.1029/2023JC019865>, 2023.



- 712 Edwards, K. F.: Mixotrophy in nanoflagellates across environmental gradients in the ocean, *Proceedings of*
713 *the National Academy of Sciences*, 116, 6211–6220, <https://doi.org/10.1073/pnas.1814860116>, 2019.
- 714 Ferronato, C., Guinder, V. A., Chidichimo, M. P., López-Abbate, C., and Amodeo, M.: Zonation of protistan
715 plankton in a productive area of the Patagonian shelf: Potential implications for the anchovy distribution,
716 *Food Webs*, 29, e00211, <https://doi.org/10.1016/j.fooweb.2021.e00211>, 2021.
- 717 Ferronato, C., Berden, G., Rivarossa, M., and Guinder, V. A.: Wind-driven currents and water masses shape
718 spring phytoplankton distribution and composition in hydrologically complex, productive shelf waters,
719 *Limnol Oceanogr*, 68, 2195–2210, <https://doi.org/10.1002/lno.12413>, 2023.
- 720 Franco, B. C., Piola, A. R., Rivas, A. L., Baldoni, A., and Pisoni, J. P.: Multiple thermal fronts near the
721 Patagonian shelf break, *Geophys Res Lett*, 35, <https://doi.org/10.1029/2007GL032066>, 2008.
- 722 Franco, B. C., Palma, E. D., Combes, V., Acha, E. M., and Saraceno, M.: Modeling the Offshore Export of
723 Subantarctic Shelf Waters From the Patagonian Shelf, *J Geophys Res Oceans*, 123, 4491–4502,
724 <https://doi.org/10.1029/2018JC013824>, 2018.
- 725 Garzón-Cardona, J. E., Guinder, V. A., Alonso, C., Martínez, A. M., Pantoja-Gutiérrez, S., Kopprio, G. A.,
726 Krock, B., and Lara, R. J.: Chemically unidentified dissolved organic carbon: A pivotal piece for microbial
727 activity in a productive area of the Northern Patagonian shelf, *Mar Environ Res*, 167, 105286,
728 <https://doi.org/10.1016/j.marenvres.2021.105286>, 2021.
- 729 Goericke, R.: The structure of marine phytoplankton communities-patterns, rules and mechanisms, *California*
730 *Cooperative Oceanic Fisheries Investigation Reports*, 52, 182–197, 2011.
- 731 Grattepanche, J.-D., McManus, G. B., and Katz, L. A.: Patchiness of Ciliate Communities Sampled at
732 Varying Spatial Scales along the New England Shelf, *PLoS One*, 11, e0167659,
733 <https://doi.org/10.1371/journal.pone.0167659>, 2016.
- 734 Gruber, D. F., Simjouw, J.-P., Seitzinger, S. P., and Taghon, G. L.: Dynamics and characterization of
735 refractory dissolved organic matter produced by a pure bacterial culture in an experimental predator-prey
736 system, *Appl Environ Microbiol*, 72, 4184–4191, <https://doi.org/10.1128/AEM.02882-05>, 2006.
- 737 Hach, P. F., Marchant, H. K., Krupke, A., Riedel, T., Meier, D. V., Lavik, G., Holtappels, M., Dittmar, T.,
738 and Kuypers, M. M. M.: Rapid microbial diversification of dissolved organic matter in oceanic surface waters
739 leads to carbon sequestration, *Sci Rep*, 10, 13025, <https://doi.org/10.1038/s41598-020-69930-y>, 2020.
- 740 Hillebrand, H., Dürselen, C., Kirschtel, D., Pollinger, U., and Zohary, T.: Biovolume calculation for pelagic
741 and benthic microalgae, *J Phycol*, 35, 403–424, <https://doi.org/10.1046/j.1529-8817.1999.3520403.x>, 1999.
- 742 Hozbor, M. C., Hernández, D. R., Cucchi Colleoni, A. D., Costagliola, M. C., and Peressutti, S. R.: Biomasa
743 y distribución espacial del bacterioplancton en el sector norte de la plataforma continental argentina (34° S-
744 41° S), *Revista de Investigación y Desarrollo Pesquero*, 23, 145–160, 2013.
- 745 Huguet, A., Vacher, L., Relexans, S., Saubusse, S., Froidefond, J. M., and Parlanti, E.: Properties of
746 fluorescent dissolved organic matter in the Gironde Estuary, *Org Geochem*, 40, 706–719,
747 <https://doi.org/10.1016/j.orggeochem.2009.03.002>, 2009.
- 748 Hutchins, D. A. and Fu, F.: Microorganisms and ocean global change, *Nat Microbiol*, 2, 17058,
749 <https://doi.org/10.1038/nmicrobiol.2017.58>, 2017.



- 750 Irigoien, X., Flynn, K. J., and Harris, R. P.: Phytoplankton blooms: a ‘loophole’ in microzooplankton grazing
751 impact?, *J Plankton Res*, 27, 313–321, <https://doi.org/10.1093/plankt/fbi011>, 2005.
- 752 Jeffrey, S. W. and Humphrey, G. F.: New spectrophotometric equations for determining chlorophylls a, b, c1
753 and c2 in higher plants, algae and natural phytoplankton, *Biochemie und Physiologie der Pflanzen*, 167, 191–
754 194, [https://doi.org/10.1016/S0015-3796\(17\)30778-3](https://doi.org/10.1016/S0015-3796(17)30778-3), 1975.
- 755 Jiao, N., Luo, T., Chen, Q., Zhao, Z., Xiao, X., Liu, J., Jian, Z., Xie, S., Thomas, H., Herndl, G. J., Benner, R.,
756 Gonsior, M., Chen, F., Cai, W.-J., and Robinson, C.: The microbial carbon pump and climate change, *Nat*
757 *Rev Microbiol*, 22, 408–419, <https://doi.org/10.1038/s41579-024-01018-0>, 2024.
- 758 Kahl, L. C., Bianchi, A. A., Osiroff, A. P., Pino, D. R., and Piola, A. R.: Distribution of sea-air CO₂ fluxes in
759 the Patagonian Sea: Seasonal, biological and thermal effects, *Cont Shelf Res*, 143, 18–28,
760 <https://doi.org/10.1016/j.csr.2017.05.011>, 2017.
- 761 Kanayama, T., Kobari, T., Suzuki, K., Yoshie, N., Honma, T., Karu, F., and Kume, G.: Impact of
762 microzooplankton grazing on the phytoplankton community in the Kuroshio of the East China sea: A major
763 trophic pathway of the Kuroshio ecosystem, *Deep Sea Research Part I: Oceanographic Research Papers*, 163,
764 103337, <https://doi.org/10.1016/j.dsr.2020.103337>, 2020.
- 765 Kang, H. C., Jeong, H. J., Ok, J. H., Lim, A. S., Lee, K., You, J. H., Park, S. A., Eom, S. H., Lee, S. Y., Lee,
766 K. H., Jang, S. H., Yoo, Y. Du, Lee, M. J., and Kim, K. Y.: Food web structure for high carbon retention in
767 marine plankton communities, *Sci Adv*, 9, <https://doi.org/10.1126/sciadv.adk0842>, 2023.
- 768 Kattner, G. and Becker, H.: Nutrients and organic nitrogenous compounds in the marginal ice zone of the
769 Fram Strait, *Journal of Marine Systems*, 2, 385–394, [https://doi.org/10.1016/0924-7963\(91\)90043-T](https://doi.org/10.1016/0924-7963(91)90043-T), 1991.
- 770 Kinsey, J. D., Corradino, G., Ziervogel, K., Schnetzer, A., and Osburn, C. L.: Formation of Chromophoric
771 Dissolved Organic Matter by Bacterial Degradation of Phytoplankton-Derived Aggregates, *Front Mar Sci*, 4,
772 <https://doi.org/10.3389/fmars.2017.00430>, 2018.
- 773 Kujawinski, E. B., Del Vecchio, R., Blough, N. V., Klein, G. C., and Marshall, A. G.: Probing molecular-
774 level transformations of dissolved organic matter: insights on photochemical degradation and protozoan
775 modification of DOM from electrospray ionization Fourier transform ion cyclotron resonance mass
776 spectrometry, *Mar Chem*, 92, 23–37, <https://doi.org/10.1016/j.marchem.2004.06.038>, 2004.
- 777 Landry, M. R. and Hassett, R. P.: Estimating the grazing impact of marine micro-zooplankton, *Mar Biol*, 67,
778 283–288, <https://doi.org/10.1007/BF00397668>, 1982.
- 779 Landry, M. R., Stukel, M. R., Selph, K. E., and Goericke, R.: Coexisting picoplankton experience different
780 relative grazing pressures across an ocean productivity gradient, *Proceedings of the National Academy of*
781 *Sciences*, 120, <https://doi.org/10.1073/pnas.2220771120>, 2023.
- 782 Laruelle, G. G., Cai, W.-J., Hu, X., Gruber, N., Mackenzie, F. T., and Regnier, P.: Continental shelves as a
783 variable but increasing global sink for atmospheric carbon dioxide, *Nat Commun*, 9, 454,
784 <https://doi.org/10.1038/s41467-017-02738-z>, 2018.
- 785 Lechtenfeld, O. J., Hertkorn, N., Shen, Y., Witt, M., and Benner, R.: Marine sequestration of carbon in
786 bacterial metabolites, *Nat Commun*, 6, 6711, <https://doi.org/10.1038/ncomms7711>, 2015.



- 787 Lee, M.-H., Osburn, C. L., Shin, K.-H., and Hur, J.: New insight into the applicability of spectroscopic indices
788 for dissolved organic matter (DOM) source discrimination in aquatic systems affected by biogeochemical
789 processes, *Water Res*, 147, 164–176, <https://doi.org/10.1016/j.watres.2018.09.048>, 2018.
- 790 Lehahn, Y., d’Ovidio, F., and Koren, I.: A Satellite-Based Lagrangian View on Phytoplankton Dynamics,
791 *Ann Rev Mar Sci*, 10, 99–119, <https://doi.org/10.1146/annurev-marine-121916-063204>, 2018.
- 792 Lønborg, C., Álvarez-Salgado, X. A., Davidson, K., Martínez-García, S., and Teira, E.: Assessing the
793 microbial bioavailability and degradation rate constants of dissolved organic matter by fluorescence
794 spectroscopy in the coastal upwelling system of the Ría de Vigo, *Mar Chem*, 119, 121–129,
795 <https://doi.org/10.1016/j.marchem.2010.02.001>, 2010.
- 796 Lønborg, C., Yokokawa, T., Herndl, G. J., and Antón Álvarez-Salgado, X.: Production and degradation of
797 fluorescent dissolved organic matter in surface waters of the eastern north Atlantic ocean, *Deep Sea Research*
798 *Part I: Oceanographic Research Papers*, 96, 28–37, <https://doi.org/10.1016/j.dsr.2014.11.001>, 2015.
- 799 Lucas, A. J., Guerrero, R. A., Mianzán, H. W., Acha, E. M., and Lasta, C. A.: Coastal oceanographic regimes
800 of the Northern Argentine Continental Shelf (34–43°S), *Estuar Coast Shelf Sci*, 65, 405–420,
801 <https://doi.org/10.1016/j.ecss.2005.06.015>, 2005.
- 802 Lund Paulsen, M., Müller, O., Larsen, A., Møller, E. F., Middelboe, M., Sejr, M. K., and Stedmon, C.:
803 Biological transformation of Arctic dissolved organic matter in a NE Greenland fjord, *Limnol Oceanogr*, 64,
804 1014–1033, <https://doi.org/10.1002/lno.11091>, 2019.
- 805 McCauley, D. J., Gellner, G., Martinez, N. D., Williams, R. J., Sandin, S. A., Micheli, F., Mumby, P. J., and
806 McCann, K. S.: On the prevalence and dynamics of inverted trophic pyramids and otherwise top-heavy
807 communities, *Ecol Lett*, 21, 439–454, <https://doi.org/10.1111/ele.12900>, 2018.
- 808 McKnight, D. M., Boyer, E. W., Westerhoff, P. K., Doran, P. T., Kulbe, T., and Andersen, D. T.:
809 Spectrofluorometric characterization of dissolved organic matter for indication of precursor organic material
810 and aromaticity, *Limnol Oceanogr*, 46, 38–48, <https://doi.org/10.4319/lo.2001.46.1.0038>, 2001.
- 811 Morán, X. A. G., Gasol, J. M., Pernice, M. C., Mangot, J., Massana, R., Lara, E., Vaqué, D., and Duarte, C.
812 M.: Temperature regulation of marine heterotrophic prokaryotes increases latitudinally as a breach between
813 bottom-up and top-down controls, *Glob Chang Biol*, 23, 3956–3964, <https://doi.org/10.1111/gcb.13730>, 2017.
- 814 Nagata, T. and Kirchman, D.: Release of macromolecular organic complexes by heterotrophic marine
815 flagellates, *Mar Ecol Prog Ser*, 83, 233–240, <https://doi.org/10.3354/meps083233>, 1992.
- 816 Negri, R. M., Silva, R. I., Segura, V., and Cucchi Colleoni, A. D.: Estructura de la comunidad del fitoplancton
817 en el área de El Rincón, Mar Argentino (febrero 2011), *Revista Investigación Desarrollo Pesquero*, 23, 7–22,
818 2013.
- 819 Negri, R. M., Molinari, G., Carignan, M., Ortega, L., Ruiz, M. G., Cozzolino, E., Cucchi-Colleoni, A. D.,
820 Lutz, V. A., Costagliola, M., Garcia, A. B., Izzo, S., Jurquiza, V., Salomone, A., Odizzio, M., La Torre, S.,
821 Sanabria, A., Hozbor, M. C., Peressutti, S. R., Méndez, S. M., Silva, R., Martínez, A., Cepeda, G. D., Viñas,
822 M. D., Diaz, M. V., Pajaro, M., Mattera, M. B., Montoya, N. G., Berghoff, C., and Leonarduzzi, E.: Ambiente
823 y plancton en la zona Común de pesca argentino-uruguayana en un escenario de cambio climático (marzo,
824 2014), *Publicaciones de la Comisión Técnica Mixta del Frente Marítimo*, 251–316, 2016.



- 825 Orselli, I. B. M., Kerr, R., Ito, R. G., Tavano, V. M., Mendes, C. R. B., and Garcia, C. A. E.: How fast is the
826 Patagonian shelf-break acidifying?, *Journal of Marine Systems*, 178, 1–14,
827 <https://doi.org/10.1016/j.jmarsys.2017.10.007>, 2018.
- 828 Osburn, C. L., Kinsey, J. D., Bianchi, T. S., and Shields, M. R.: Formation of planktonic chromophoric
829 dissolved organic matter in the ocean, *Mar Chem*, 209, 1–13, <https://doi.org/10.1016/j.marchem.2018.11.010>,
830 2019.
- 831 Pasulka, A. L., Samo, T. J., and Landry, M. R.: Grazer and viral impacts on microbial growth and mortality in
832 the southern California Current Ecosystem, *J Plankton Res*, 37, 320–336,
833 <https://doi.org/10.1093/plankt/fbv011>, 2015.
- 834 Péquin, B., LaBrie, R., St-Gelais, N. F., and Maranger, R.: Succession of protistan functional traits is
835 influenced by bloom timing, *Front Mar Sci*, 9, <https://doi.org/10.3389/fmars.2022.916093>, 2022.
- 836 Porter, K. G. and Feig, Y. S.: The use of DAPI for identifying and counting aquatic microflora, *Limnol*
837 *Oceanogr*, 25, 943–948, <https://doi.org/10.4319/lo.1980.25.5.0943>, 1980.
- 838 Proctor, L. and Fuhrman, J.: Roles of viral infection in organic particle flux, *Mar Ecol Prog Ser*, 69, 133–142,
839 <https://doi.org/10.3354/meps069133>, 1991.
- 840 Redfield, A. C., Ketchum, B. H., and Richards, F. A.: The influence of organisms on the composition of sea-
841 water, in: *The sea: ideas and observations on progress in the study of the seas*, vol. 2, edited by: Hill, M. N.,
842 Wiley Interscience, New York, 26–77, 1963.
- 843 Romera Castillo, C., Sarmiento, H., Álvarez-Salgado, X. A., Gasol, J. M., and Marrasé, C.: Production of
844 chromophoric dissolved organic matter by marine phytoplankton, *Limnol Oceanogr*, 55, 446–454,
845 <https://doi.org/10.4319/lo.2010.55.1.0446>, 2010.
- 846 Romera-Castillo, C., Sarmiento, H., Álvarez-Salgado, X. A., Gasol, J. M., and Marrasé, C.: Net Production
847 and Consumption of Fluorescent Colored Dissolved Organic Matter by Natural Bacterial Assemblages
848 Growing on Marine Phytoplankton Exudates, *Appl Environ Microbiol*, 77, 7490–7498,
849 <https://doi.org/10.1128/AEM.00200-11>, 2011.
- 850 Romero, S. I., Piola, A. R., Charo, M., and Garcia, C. a. E.: Chlorophyll- a variability off Patagonia based on
851 SeaWiFS data, *J Geophys Res*, 111, 1–11, <https://doi.org/10.1029/2005JC003244>, 2006.
- 852 Sanders, R., Caron, D., and Berninger U, G.: Relationships between bacteria and heterotrophic nanoplankton
853 in marine and fresh waters: an inter-ecosystem comparison, *Mar Ecol Prog Ser*, 86, 1–14,
854 <https://doi.org/10.3354/meps086001>, 1992.
- 855 Saraceno, M., Bodnariuk, N., Ruiz-Etcheverry, L. A., Berta, M., Simionato, C. G., Beron-Vera, F. J., and
856 Olascoaga, M. J.: Lagrangian characterization of the southwestern Atlantic from a dense surface drifter
857 deployment, *Deep Sea Research Part I: Oceanographic Research Papers*, 208, 104319,
858 <https://doi.org/10.1016/j.dsr.2024.104319>, 2024.
- 859 Sarmiento, H., Morana, C., and Gasol, J. M.: Bacterioplankton niche partitioning in the use of phytoplankton-
860 derived dissolved organic carbon: quantity is more important than quality, *ISME J*, 10, 2582–2592,
861 <https://doi.org/10.1038/ismej.2016.66>, 2016.



- 862 Schloss, I., Ferreyra, G., Ferrario, M., Almandoz, G., Codina, R., Bianchi, A., Balestrini, C., Ochoa, H., Ruiz
863 Pino, D., and Poisson, A.: Role of plankton communities in sea-air variations in pCO₂ in the SW Atlantic
864 Ocean, *Mar Ecol Prog Ser*, 332, 93–106, <https://doi.org/10.3354/meps332093>, 2007.
- 865 Sherr, E. B. and Sherr, B. F.: Phagotrophic Protists: Central Roles in Microbial Food Webs, in: *Aquatic
866 Microbial Ecology and Biogeochemistry: A Dual Perspective*, Springer International Publishing, Cham, 3–12,
867 https://doi.org/10.1007/978-3-319-30259-1_1, 2016.
- 868 Silva, R., Negri, R., and Lutz, V.: Summer succession of ultraphytoplankton at the EPEA coastal station
869 (Northern Argentina), *J Plankton Res*, 31, 447–458, <https://doi.org/10.1093/plankt/fbn128>, 2009.
- 870 Simon, M. and Azam, F.: Protein content and protein synthesis rates of planktonic marine bacteria, *Mar Ecol
871 Prog Ser*, 51, 201–213, <https://doi.org/10.3354/meps051201>, 1989.
- 872 Skoog, A., Thomas, D., Lara, R., and Richter, K.-U.: Methodological investigations on DOC determinations
873 by the HTCO method, *Mar Chem*, 56, 39–44, [https://doi.org/10.1016/S0304-4203\(96\)00084-9](https://doi.org/10.1016/S0304-4203(96)00084-9), 1997.
- 874 Snyder, R. A., Moss, J. A., Santoferrara, L., Head, M., and Jeffrey, W. H.: Ciliate microzooplankton from the
875 Northeastern Gulf of Mexico, *ICES Journal of Marine Science*, 78, 3356–3371,
876 <https://doi.org/10.1093/icesjms/fsab002>, 2021.
- 877 Spencer, R. G. M., Pellerin, B. A., Bergamaschi, B. A., Downing, B. D., Kraus, T. E. C., Smart, D. R.,
878 Dahlgren, R. A., and Hernes, P. J.: Diurnal variability in riverine dissolved organic matter composition
879 determined by *in situ* optical measurement in the San Joaquin River (California, USA), *Hydrol Process*, 21,
880 3181–3189, <https://doi.org/10.1002/hyp.6887>, 2007.
- 881 Stedmon, C. A. and Bro, R.: Characterizing dissolved organic matter fluorescence with parallel factor
882 analysis: a tutorial, *Limnol Oceanogr Methods*, 6, 572–579, <https://doi.org/10.4319/lom.2008.6.572>, 2008.
- 883 Suttle, C. A.: Viruses in the sea, *Nature*, 437, 356–361, <https://doi.org/10.1038/nature04160>, 2005.
- 884 Taylor, A. and Landry, M.: Phytoplankton biomass and size structure across trophic gradients in the southern
885 California Current and adjacent ocean ecosystems, *Mar Ecol Prog Ser*, 592, 1–17,
886 <https://doi.org/10.3354/meps12526>, 2018a.
- 887 Taylor, A. and Landry, M.: Phytoplankton biomass and size structure across trophic gradients in the southern
888 California Current and adjacent ocean ecosystems, *Mar Ecol Prog Ser*, 592, 1–17,
889 <https://doi.org/10.3354/meps12526>, 2018b.
- 890 Taylor, G. T., Iturriaga, R., and Sullivan, C. W.: Interactions of bacterivorous grazers and heterotrophic bacteria
891 with dissolved organic matter, *Mar. Ecol. Prog. Ser.*, 60, 1884–1888, 1985.
- 892 Timko, S. A., Maydanov, A., Pittelli, S. L., Conte, M. H., Cooper, W. J., Koch, B. P., Schmitt-Kopplin, P.,
893 and Gonsior, M.: Depth-dependent photodegradation of marine dissolved organic matter, *Front Mar Sci*, 2,
894 <https://doi.org/10.3389/fmars.2015.00066>, 2015.
- 895 Tremaine, S. C. and Mills, A. L.: Tests of the Critical Assumptions of the Dilution Method for Estimating
896 Bacterivory by Microeucaryotes, *Appl Environ Microbiol*, 53, 2914–2921,
897 <https://doi.org/10.1128/aem.53.12.2914-2921.1987>, 1987.
- 898 Urban-Rich, J., McCarty, J. T., and Shailer, M.: Effects of food concentration and diet on chromophoric
899 dissolved organic matter accumulation and fluorescent composition during grazing experiments with the



900 copepod *Calanus finmarchicus*, *ICES Journal of Marine Science*, 61, 542–551,
901 <https://doi.org/10.1016/j.icesjms.2004.03.024>, 2004.
902 Ward, B. A. and Follows, M. J.: Marine mixotrophy increases trophic transfer efficiency, mean organism size,
903 and vertical carbon flux, *Proceedings of the National Academy of Sciences*, 113, 2958–2963,
904 <https://doi.org/10.1073/pnas.1517118113>, 2016.
905 Weinbauer, M. G. and Peduzzi, P.: Significance of viruses versus heterotrophic nanoflagellates for controlling
906 bacterial abundance in the northern Adriatic Sea, *J Plankton Res*, 17, 1851–1856,
907 <https://doi.org/10.1093/plankt/17.9.1851>, 1995.
908 Weisse, T., Anderson, R., Arndt, H., Calbet, A., Hansen, P. J., and Montagnes, D. J. S.: Functional ecology of
909 aquatic phagotrophic protists – Concepts, limitations, and perspectives, *Eur J Protistol*, 55, 50–74,
910 <https://doi.org/10.1016/j.ejop.2016.03.003>, 2016.
911 Zhao, Z., Li, H., Sun, Y., Shao, K., Wang, X., Ma, X., Hu, A., Zhang, H., and Fan, J.: How habitat
912 heterogeneity shapes bacterial and protistan communities in temperate coastal areas near estuaries, *Environ*
913 *Microbiol*, 24, 1775–1789, <https://doi.org/10.1111/1462-2920.15892>, 2022.
914 Zheng, Q., Chen, Q., Cai, R., He, C., Guo, W., Wang, Y., Shi, Q., Chen, C., and Jiao, N.: Molecular
915 characteristics of microbially mediated transformations of *Synechococcus*-derived dissolved organic matter as
916 revealed by incubation experiments, *Environ Microbiol*, 21, 2533–2543, [https://doi.org/10.1111/1462-](https://doi.org/10.1111/1462-2920.14646)
917 [2920.14646](https://doi.org/10.1111/1462-2920.14646), 2019.
918